ACS Energy LETTERS

http://pubs.acs.org/journal/aelccp

Reduction of Hole Carriers by van der Waals Contact for Enhanced Photoluminescence Quantum Yield in Two-Dimensional Tin Halide Perovskite

Jun-Ho Park, Youjin Reo, Ju-Hyun Jung, Taehyun Kim, Taiho Park, Yong-Young Noh,* and Cheol-Joo Kim*

Cite This: *ACS Energy Lett.* 2023, 8, 3536−3544

Read Online

ACCESS | Metrics & More | Article Recommendations | Supporting Information

ABSTRACT: The role of electronic doping in determining the luminescence efficiency of low-dimensional halide perovskites has been challenging to test due to the structural complexity resulting from conventional dopant use. In this study, we demonstrate that van der Waals contact of aluminum (Al) onto a two-dimensional tin halide perovskite, phenethylammonium tin iodide (PEA_2SnI_4), enhances photoluminescence (PL) intensity significantly, reaching a record-high PL quantum yield of 10%. The intensity relies on the contact metal type and reverts when the contact is released, demonstrating structural invariability. Ultraviolet photoemission spectroscopy reveals a 0.6 eV Fermi-level upshift caused by the Al contact, indicating a reduced hole concentration. Incident power-dependence and time-resolved PL suggest trap-assisted recombination as the primary nonradiative pathway. The Shockley-Read-Hall theory predicts suppression of trap-assisted recombination due to reduced free carrier concentration, providing a quantitative explanation for our findings. Our study emphasizes the significance of controlling electronic doping to optimize luminescence efficiency in low-dimensional perovskites.

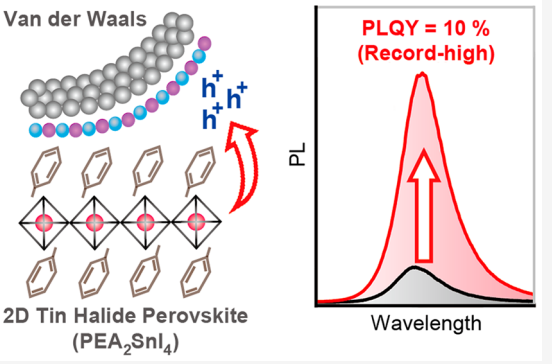

Halide perovskites have attracted significant attention as emerging emissive materials due to their direct band gaps and solution-based production methods. Low-dimensional perovskite structures, such as quantum dots and layered structures,[1−3] can be synthesized to enhance the fluorescence quantum yield (QY) by spatially confining excess carriers,[4] which exhibit high diffusivity in three-dimensional cases.[5] However, the low-dimensional structures with large surface areas are prone to hosting defect structures, such as undercoordinated atoms, impurities, and vacancies.[6] While defect states are known to exist at shallow energy levels in three-dimensional lead-based perovskites, which make the materials defect-tolerant,[7] recent studies have shown that defect states still form at deep levels in nanocrystalline structures.[8−10] Additionally, there is a growing demand for nontoxic, nonlead perovskites, such as tin-based perovskites,[11,12] which typically exhibit significantly higher defect densities than lead perovskites due to the low formation energy of defects. Therefore, engineering perovskite materials to suppress the formation of defects[13,14] and/or deactivate the defect states,[15,16] which often act as nonradiative recombination pathways and limit the QY values, is at the heart of developments for efficient light-emitting materials and devices.[6,17]

A useful approach for manipulating defect states in perovskites is to incorporate chemical additives during or after growth. These additives can include molecular ligands that passivate undercoordinated atoms[18] and reducing agents that hinder defect formation through oxidation.[19] While these approaches have led to noticeable improvements in fluorescence QY, the mechanisms responsible for these effects are not fully understood in all cases, as chemical additives can also

Received: June 16, 2023
Accepted: July 25, 2023

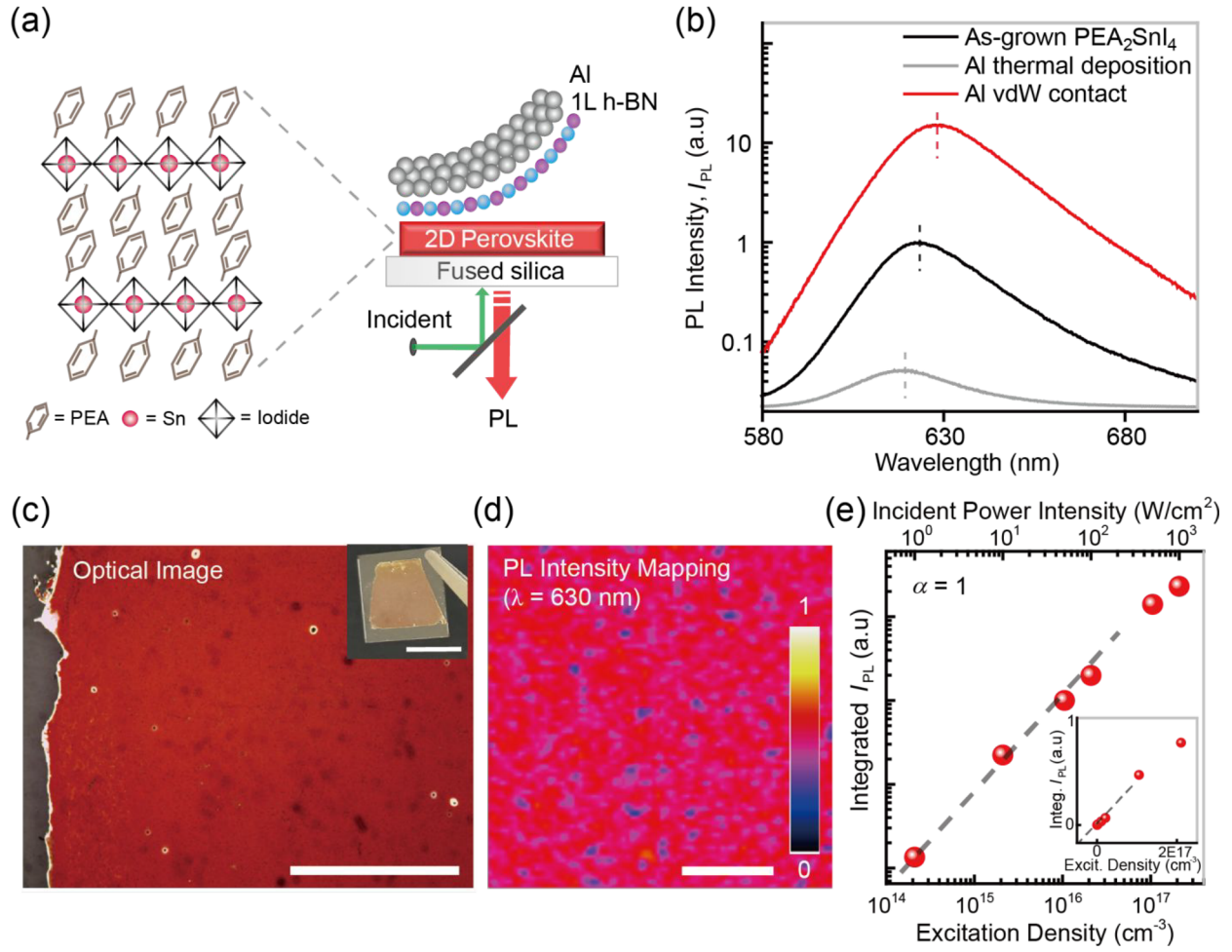

Figure 1. (a) Crystalline structure of the PEA_2SnI_4 film (left). Schematics for PL measurements on the PEA_2SnI_4 film with vdW Al contact (right). (b) Relative PL intensity (I_{PL}) spectra for as-grown (black), Al-evaporated (gray), and vdW Al-contacted PEA_2SnI_4 films (red). The power density of the excitation laser of 532 nm in wavelength is 50 W/cm^2. (c) Optical reflectance image of the PEA_2SnI_4 film after the vdW contact. Scale bar: 1 mm. (inset) Photograph of the same sample. Scale bar: 1 cm. (d) I_{PL} mapping image of the sample in (c). Scale bar: 20 μm. (e) Integrated I_{PL} as a function of the incident laser power.

have additional effects on the physical properties of the material.

The alteration of the perovskite doping levels through charge transfer between additives and perovskites is a key example. The concentration of free carriers can significantly influence the yield of various relaxation processes for excited carriers, including exciton recombination,[20,21] Auger recombination, and Shockley-Read-Hall (SRH) recombination,[22] ultimately determining the overall fluorescence QY. Understanding the primary relaxation pathway for a specific perovskite and investigating how the concentration of free carriers affects these pathways will be valuable in developing strategies to enhance the fluorescence QY of the material. While there have been some reports on the luminescence properties of halide perovskites influenced by the electronic doping effect through the adsorption of molecular[16,19,23,24] or ionic dopants[23−25] onto perovskites, the introduction of foreign dopants often leads to diffusion into the soft perovskite lattices, resulting in changes in chemical structures, including the density of atomic defects such as vacancies and grain structures.[19,25,26] Moreover, the addition of extra solvents to introduce dopants can also modify the structure of the target material, particularly for halide perovskites that are highly sensitive to solvent environment changes.[27−29] Consequently, investigating the precise role of electronic doping effects on the relaxation processes of excited carriers remains a challenge.[23]

Here, we introduce all-dry van der Waals (vdW) contacts of metallic films onto perovskites to electronically dope the materials through charge transfer between perovskites and metals with different electrochemical potentials. We selected two-dimensional (2D) phenethylammonium tin iodide (PEA_2SnI_4) perovskites as representative nontoxic, lead-free materials[11,12] known for their strongly confined excitonic features and high luminescence QY.[30,31] We confirmed that the doping level of 2D PEA_2SnI_4 significantly changes depending on the types of metals in contact, while the perovskite structures remained intact. Notably, the photoluminescence (PL) intensity was significantly enhanced after the vdW contact with aluminum films. This transformation changed the originally *p*-type doped 2D perovskite, which had high densities of defect states,[32] to an electronically intrinsic state, thereby demonstrating the crucial role of electronic doping in the relaxation processes of excited carriers.

The 2D perovskite structure and the PL measurement scheme are illustrated in Figure 1a (see the Experimental Section for detailed information). PEA_2SnI_4 thin films were

https://doi.org/10.1021/acsenergylett.3c01195
ACS Energy Lett. 2023, 8, 3536−3544

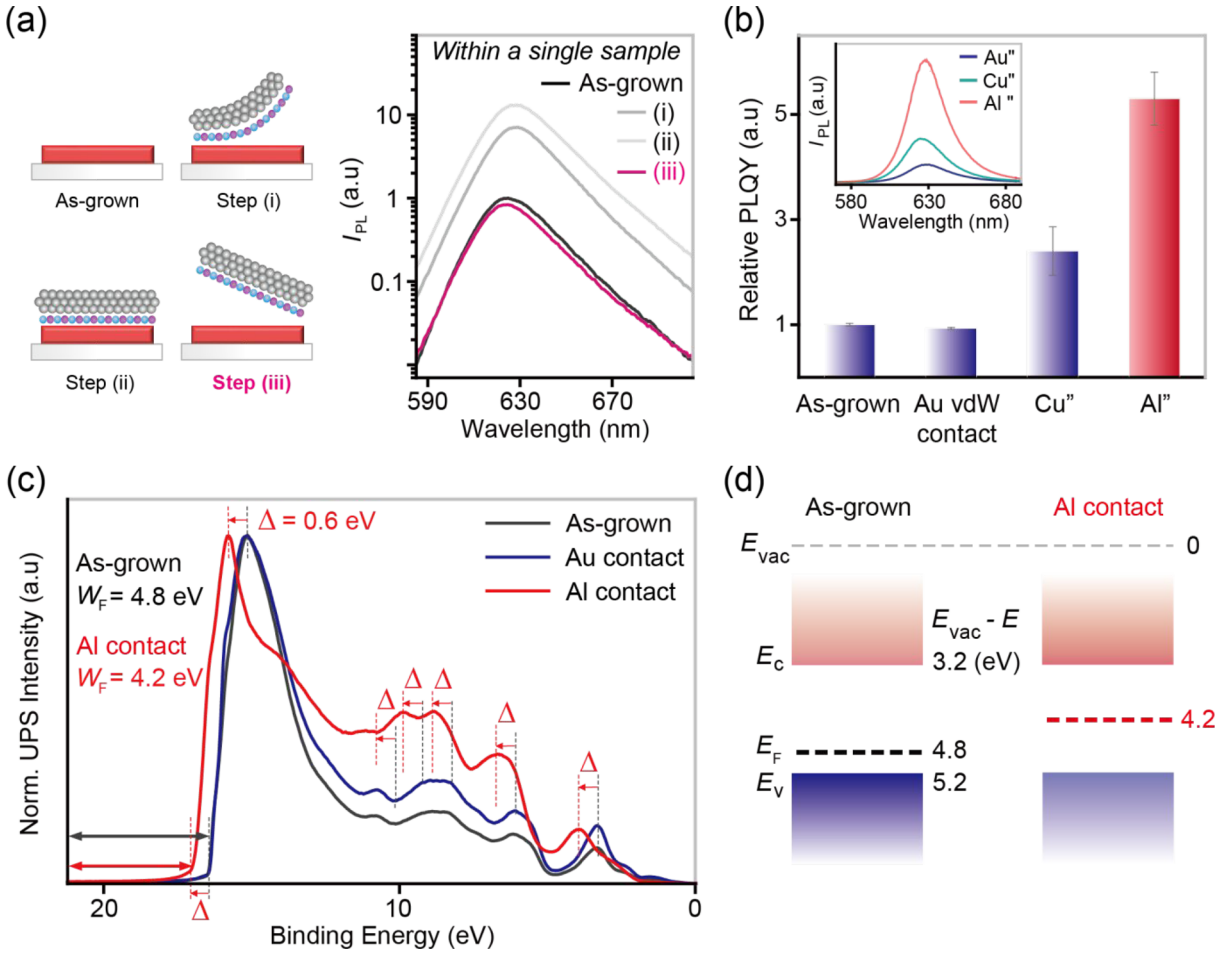

Figure 2. (a) Schematics for subsequent vdW contact and detachment of the Al film onto the PEA_2SnI_4 thin film (left). I_{PL} spectra at each step in the left schematics (right). (b) Relative PLQY of PEA_2SnI_4 with a vdW contact of different metals. The inset shows I_{PL} spectra of the samples. (c) Normalized intensity spectra by UPS from the PEA_2SnI_4 on three different substrates (fused silica, Au, and Al). The W_F values were determined as the difference between the secondary cutoff energy and the incident UV energy of 21.22 eV. The dotted lines indicate the intensity peaks and saddle points, which are shifted by 0.6 eV between PEA_2SnI_4 on Au and PEA_2SnI_4 on Al. (d) Band structures of as-grown and Al-contacted PEA_2SnI_4. The E_F values were deduced from the UPS measurements in (c), and the E_c and E_v were taken from a reference.[31]

grown on optically transparent fused silica substrates using a solution process.[33,34] X-ray diffraction (XRD) and UV−vis absorption spectra (Figure S1) confirmed that the crystalline orientation was entirely parallel to the substrates, following a layer-by-layer structure. The metallic films for vdW contact were formed on monolayer hexagonal boron nitride (1L h-BN)/germanium (Ge) substrates by thermal evaporation. Since the interfacial interactions between h-BN and Ge are weak,[35] the metallic films can be mechanically detached along with the underlying 1L h-BN and transferred onto the perovskite surface (refer to the schematic procedure in Figure S2). Subsequently, the metal/1L h-BN/perovskite structure was flipped over, and PL measurements were conducted by using a reflection beam geometry (Figure 1a).

The PL intensity after the vdW contact of aluminum (Al)/1L h-BN (Figure 1b) became significantly higher than that of the as-grown perovskite, surpassing it by more than an order of magnitude. The reflection from the metal underneath increases both the absorption of incident light and the PL collection efficiency (Figures S3−5, Table S1). However, the observed PL increase was beyond expectation, indicating that there is an additional factor contributing to the enhanced PL. We also observed that the PL intensity greatly reduced when a thin Al_2O_3 layer was inserted between Al and the perovskite film while maintaining the same reflectance geometry (Figure S6). While the PL peak shifted between samples, the shift was insignificant, as 10 meV in photon energy, indicating that the optical band gaps are similar (Figure S7 with the discussion on the possible reasons for the peak shifts). Moreover, the surface of the PEA_2SnI_4 film, taken through the fused silica, maintained its original red color uniformly across the entire surface (Figure 1c) and exhibited consistent PL intensities (Figure 1d). Both XRD (Figure S1a) and optical ellipsometry (Figures S3 and S4) measurements confirmed that our vdW contact process did not cause any structural changes in the perovskite. In contrast, when aluminum was directly evaporated onto the as-grown perovskite, the PL intensity was greatly reduced to 0.04 times the original intensity (Figure 1b), suggesting structural damage to the soft perovskite lattice caused by the evaporation of hot metals.[36] The PL intensity showed a power-law-dependence on the incident power density with a constant exponent, α = 1 (Figure 1e). The extrapolated data line passes through the origin, confirming that constant α is maintained across the entire range of low

https://doi.org/10.1021/acsenergylett.3c01195
ACS Energy Lett. 2023, 8, 3536−3544

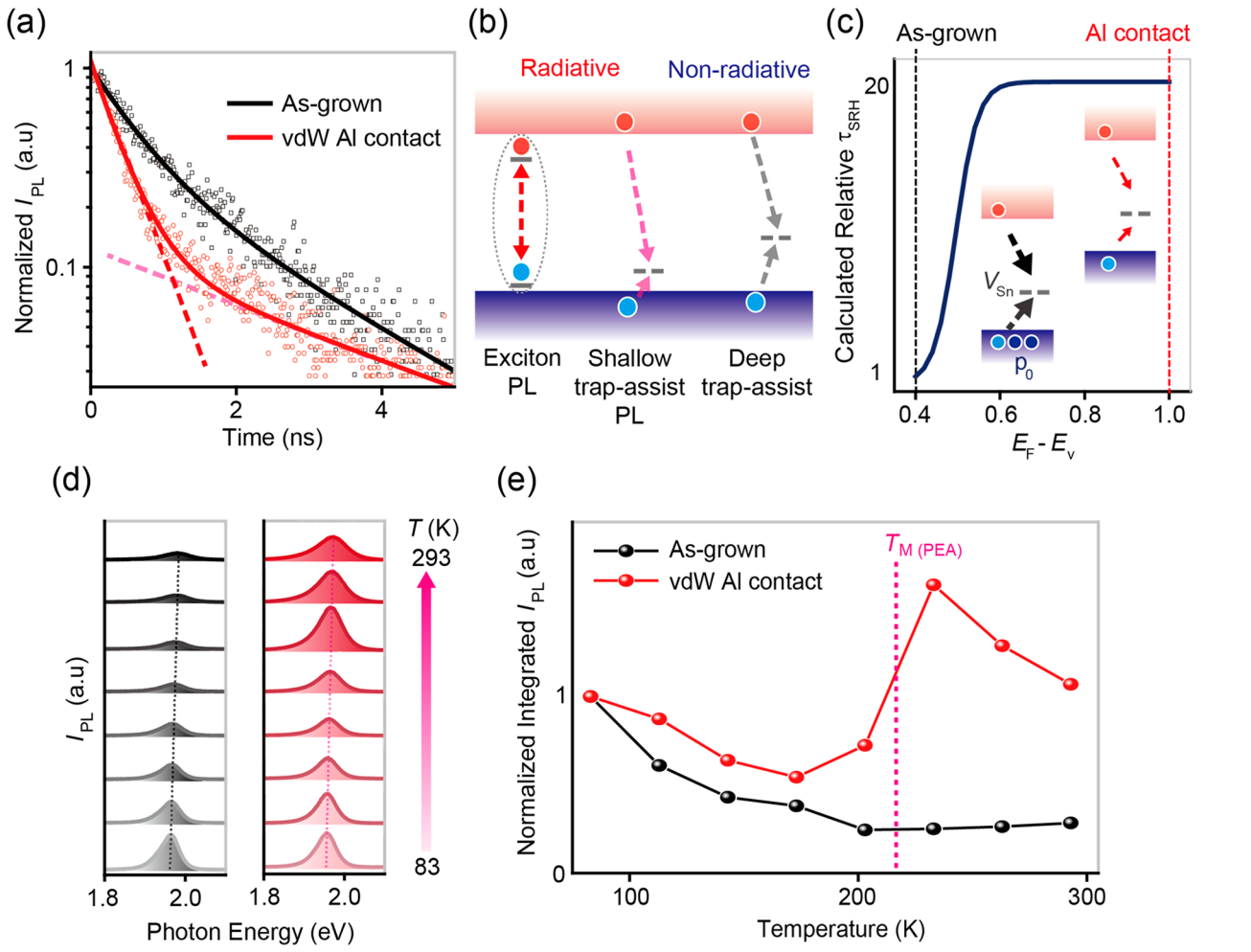

Figure 3. (a) TRPL data for as-grown (black squares) and vdW Al-contacted PEA_2SnI_4 (red circles). (b) Schematics for three different pathways for electron−hole recombination, including exciton recombination and shallow and deep trap-assisted recombination (from left to right). (c) Calculated SRH relative lifetime, assisted by V_{Sn} trap states,[43] as a function of (E_F − E_V) of the PEA_2SnI_4 at the thermal equilibrium state. Black and red dotted lines on the data indicate the measured E_F for as-grown and Al-contacted samples, respectively. The inset schematics illustrate the nonradiative recombination for each case. (d) Temperature (T)-dependent PL spectra of as-grown (left, black) and vdW Al-contacted PEA_2SnI_4 (right, red). (e) Integrated PL intensity versus T obtained from the data in (d). $T_{M(PEA)}$ indicates the melting T of PEA.

incident power in our measurements (Figure 1e, inset). While the band-to-band recombination model, without considering excitons, predicts $\alpha > 1$ with nonmonotonic changes,[37] the constant $\alpha \approx 1$ observed suggests the presence of exciton-related relaxations. This is expected due to the high exciton binding energy (130 meV)[30] compared to the thermal energy (25 meV) in this quantum-confined Ruddlesden−Popper perovskite structure.

We further confirmed the correlation between the PL intensity and the vdW contact by measuring the PL intensity during the subsequent adhesion and detachment of Al/1L h-BN on the same perovskite (Figure 2a). The Al vdW contact at step (i) immediately enhanced the PL intensity, and the PL signals gradually increased during step (ii) as a result of post-annealing, which induced conformal contacts of the Al superlayer. Importantly, after step (iii), where the vdW contact was released by mechanical detachment, the PL intensity returned to the original value of the as-grown sample. This observation suggests that our vdW contact process did not alter the chemical structure of the 2D perovskite, as also evidenced by the unchanged structural parameters and optical refractive index upon Al contact (Figures S1a, S3). To identify the reason for the enhanced PL intensity, we examined the change in the relative PL quantum yield (PLQY) resulting from the vdW contact of different metal films, including gold (Au) and copper (Cu), as shown in Figure 2b. The relative PLQY was determined by calculating the ratio of the emitted PL to the absorbed incident light (for detailed measurement procedures, refer to Figures S3−5 and Table S1). The PLQY exhibited a strong correlation with the type of metal in contact. It increased by a factor of 5 when in contact with Al and a factor of 2 when in contact with Cu. However, when in contact with Au, the PLQY remained similar to the value of the as-grown sample. A previous study has shown that the vdW contact of different metals on semiconductors can effectively modulate the Fermi level (E_F) of the semiconductor through charge transfers, without inducing significant pinning states at the interface.[36,38,39] To investigate this possibility, we performed ultraviolet photoemission spectroscopy (UPS) on the PEA_2SnI_4 films with Au and Al contacts as well as without any metal contact (Figure 2c, see Methods for details). The positions of all local peak extrema, including peaks and saddle

https://doi.org/10.1021/acsenergylett.3c01195
ACS Energy Lett. 2023, 8, 3536−3544

points, in the UPS data from the sample with Au contact (black line) and without any contact (blue line) coincide with each other. However, all of the positions of the extrema shifted by 0.6 eV with the Al contact, as indicated by the dotted lines in the graph. The work functions (W_F) were determined as 4.8 and 4.2 eV for the as-grown and Al-contacted samples, respectively, based on the energy difference between the secondary electron cutoff and the binding energy of the incident photon (21.22 eV). The UPS signals near the valence band edge were too small to deduce a reliable estimation of the energy levels; therefore, we used the reported energy levels for the conduction and valence band edges of PEA_2SnI_4 from a previous study.[31] The as-grown and Au-contacted samples exhibit *p*-type band alignments, which are consistent with their electrical properties.[32] However, the Al-contacted film shows an intrinsic alignment (Figure 2d).

PEA_2SnI_4 is known to host abundant Sn^{4+} states due to the low oxidation energy barrier, which results in a high density of defects acting as acceptors.[40] Our data indicate that the free hole carriers were effectively removed to Al, which has a low work function. It is noteworthy that the UPS experiment was conducted on the exposed surface of the PEA_2SnI_4 film, opposite the metal-contacted plane. The thin geometry of the PEA_2SnI_4 film, which was measured to be 65 nm thick by ellipsometry (Figure S3), may have facilitated charge transfer across the entire film thickness. The significant change in the doping level suggests that the concentration of free carriers plays a key role in determining the PLQY in 2D PEA_2SnI_4.

To understand how the doping level changes the dynamics of photoexcited carriers, we conducted time-resolved PL (TRPL) measurements on both the as-grown sample (Figure 3a, black square) and the sample with vdW Al contact (red circle). The change in the PL signal over time in both samples follows a biexponential decay, as depicted by the two extrapolated lines in Figure 3a. Significantly, the time constant for the fast decay was reduced from 0.6 ns in the as-grown sample to 0.4 ns in the sample with Al contact, while the time constant for the slow decay increased with Al contact (see Table S2 for detailed fitting results). The presence of two independent decays indicates that there are two different sources of PL emission. Previous studies have shown that the fast PL decay is dominated by direct exciton recombination, while the later PL decay is associated with shallow trap-assisted recombination[41] (schematics in Figure 3b). The faster exciton recombination rates in the sample with Al contact can be attributed to a reduced charge-blocking effect resulting from a reduced free carrier concentration.[42] However, the observed enhancement in the exciton recombination rate by 1.5 times alone cannot explain the 5-fold increase in PLQY, suggesting that nonradiative recombination losses should also be reduced. We have considered two different mechanisms of recombination as potential nonradiative relaxation pathways in this system, including Auger and trap-assisted recombination. The Auger recombination rate is proportional to $(\Delta n)^3$ in the high-level injection condition where Δn is the excited electron (or hole) concentration. Since the exciton recombination rate is proportional to Δn, the PLQY is expected to rapidly decline as Δn increases.[22] However, the PLQY shows near independence from Δn, with an α value close to unity at the high-level injection condition in Figure 1e, where Δn exceeds the free carrier concentrations in the dark states (see the recombination model in the Supporting Information). This suggests that Auger recombination is not the main nonradiative relaxation pathway. On the other hand, the trap-assisted recombination rate through in-gap states is proportional to Δn in the high-level condition, resulting in Δn-independent PLQY,[22] which is consistent with our observations in Figure 1e.

To quantitatively analyze how the trap-assisted recombination rate changes between perovskites with different E_F levels (Figure 2d), we deduced the recombination lifetime, τ_{SRH}, as a function of free carrier concentrations at the dark state based on SRH theory (see Supporting Information for the detailed calculations). The major trap states are assumed to be the abundant Sn vacancy states, V_{Sn}, whose relative energy level within the band gap has been calculated elsewhere.[43] For an excitation density of 10^{16} cm^{-3} at steady state, τ_{SRH} increases significantly from the as-grown sample with E_F close to the valence band edge, E_V, at the dark state (represented by the dotted black line) to the sample with vdW Al contact with E_F close to the midgap (represented by the dotted red line), by approximately 20 times (Figure 3c). The hole concentration at thermal equilibrium state, p_0, in the as-grown sample is extracted from Hall measurements in a previous study,[33] yielding a value of 4×10^{17} cm^{-3}. The p_0 value is much higher than the excitation density in our measurements (Figure 1e), representing a low-level injection condition. In the low-level injection condition, where the minority carrier capturing process dominates the entire relaxation process, τ_{SRH} is typically lower compared to the high-level condition, where both electron and hole capturing processes are important to determine the total τ_{SRH} (see Supporting Information for a detailed discussion). In summary, our analytic model suggests that it is crucial to reduce p_0 below Δn to minimize trap-assisted recombination via existing in-gap states.

One may note that in a quantum-confined system, photoexcited carriers predominantly form bound excitons, and the recombination rate through these bound states does not significantly depend on the electronic doping concentration.[37] However, strong electron−phonon coupling in the soft perovskite lattice[44] can also facilitate the trap-assisted recombination of photocarriers.[45,46] We also note that if the radiative recombination results from free carriers rather than bound excitons, as in the case of most 3D systems, reducing p_0 will also decrease the radiative recombination rate, and the enhancement of PLQY will not occur. Therefore, the enhanced PL due to the suppression of free carrier concentrations would only be relevant in low-dimensional materials with efficient formation of radiative excitons.

To further investigate the effect of phonons on the PLQY, we observed the luminescence while decreasing the temperature of the samples (Figure 3d,e). Both the samples with and without Al contact exhibited a red-shift of the PL peak energy as the temperature decreased, which is consistent with a previous report[47] and suggests strong electron−phonon coupling.[48] The PL intensities in the Al-contacted sample increased as the temperature decreased from room temperature, then suddenly dropped near 210 K, and increased again down to 90 K. We attribute the initial enhancement of PLQY when the temperature decreased below room temperature to the suppression of thermal exciton dissociation. This tendency can be particularly prominent when other nonradiative relaxation pathways, such as trap-assisted recombination, are already suppressed with the presence of Al contact. We found that suppressed PL below 210 K was irreversible. Considering that the transition temperature is close to the melting temperature of organic PEA,[49] we speculate that structural

https://doi.org/10.1021/acsenergylett.3c01195
ACS Energy Lett. 2023, 8, 3536−3544

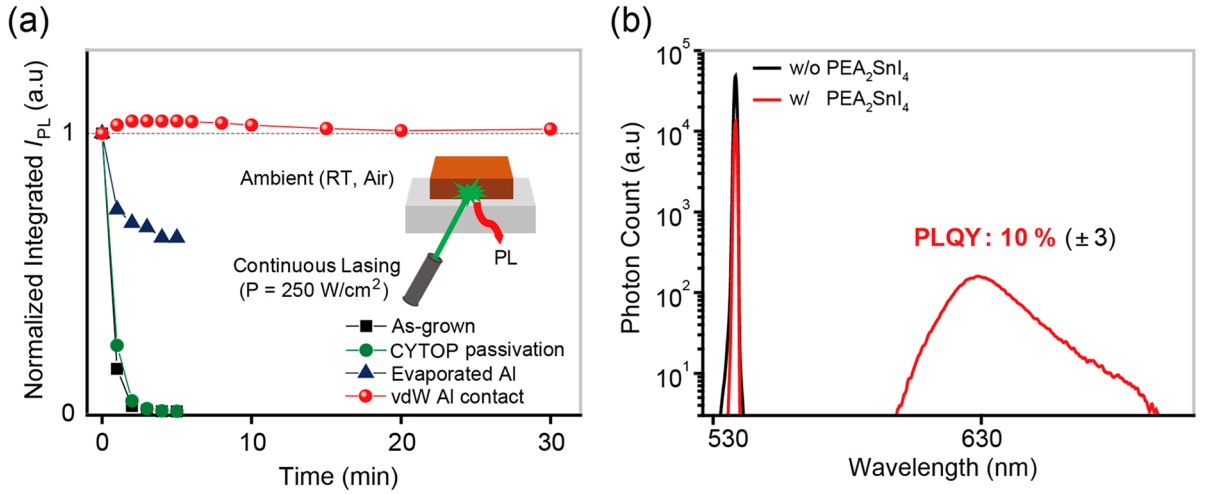

Figure 4. (a) Normalized integrated PL intensity as a function of the excitation time with a continuous 532 nm laser at 250 W/cm^2 in an ambient environment. As-grown PEA_2SnI_4 film and those with three different overlayers (CYTOP, thermally evaporated Al, vdW-contacted Al) were tested. (b) Spectra of reflected lights with PEA_2SnI_4/vdW-contacted Al (red) and with only Al surface without PEA_2SnI_4 (black) to deduce absolute PLQY by comparing absorbed incident lights near 532 nm and emitted PL near 630 nm.

deformations occurred during the solidification of the PEA layer, inducing more trap states in the emitting inorganic layer.

Lastly, we tested how the vdW metal contact enhances the stability of materials in maintaining the PL upon photoexcitation. The material stability is important for reliable device operations based on tin-based perovskites as successfully demonstrated in previous studies.[12,50] As shown in Figure 4a, the PL from the sample with vdW Al contact exhibited a constant intensity under continuous injection of a high-power laser (= 250 W/cm^2) in ambient conditions. In contrast, the PL signals quickly decreased in the as-grown sample as well as in the sample protected by a typical passivation material of cyclized transparent optical polymer (CYTOP). Photoexcited carriers can facilitate the oxidation of perovskite, resulting in the suppression of PL.[40] Efficient relaxation of photocarriers (Figure 3a) and the conformal vdW contact with the high-quality metal film to block oxygen diffusion into the perovskite could be the reason for the high stability. In particular, the vdW contact protects the perovskite from photoinduced oxidation better than the directly evaporated metal, suggesting that the deposited metal on h-BN would have an excellent crystalline structure with low oxygen diffusivity.

The absolute PLQY from the sample with the vdW contact of Al was estimated from the ratio between the emitted PL photons and the absorbed incident photons (Figure 4b) (see Figure S8 for a validation of the measurement method). A record-high value of 10% for PEA_2SnI_4 was deduced. Previous strategies to achieve a high PLQY (see Table S3 for detailed information) have mostly focused on modifying the chemical structures,[6] but we have demonstrated that electrical tuning without altering the chemical structure can still significantly enhance the PLQY. This finding provides a key clue for selecting interlayer materials in the architectures of light-emitting devices that contact the emitting perovskite layer. Additionally, for the synthesis of perovskites, our result implies that the electronegativity of additives must be carefully considered. Previous studies have indeed shown that molecular additives, such as surface passivating molecules, can significantly change the overall electronic doping level.[18] In this study, the vdW metal contact demonstrated significant enhancement of PL, despite the potential quenching through diffusion of photocarriers toward the metal. While exciton diffusion within the short exciton lifetime[41,51] is suppressed due to the existence of additional interlayers,[52,53] the use of insulating molecules for modulation of electrical doping can further improve the PLQY for low-dimensional perovskites with abundant trap states.

EXPERIMENTAL SECTION

Sample Preparations. PEA_2SnI_4 thin film was prepared on a fused silica substrate by spin-coating using mixed PEAI and SnI_2 precursor solution in a glovebox, following the detailed recipe from the previous study.[33,34]

To prepare metal films for the vdW contacts, 1L h-BN was first grown on polished Ge (110) substrates using chemical vapor deposition with borazine precursors as described in a previous study.[35] Target metals (Al, Cu, or Au) were thermally evaporated onto the as-grown 1L h-BN/Ge substrates with a thickness of 40 nm and a deposition rate of 0.5 Å/s in a high-vacuum chamber (~10^{-6} Torr). A poly(methyl methacrylate) (PMMA) solution (996 K, 8% in anisole) was spin-coated onto the metallic film. A thermal release tape (TRT) was attached onto the PMMA surface and then lifted to mechanically exfoliate the PMMA/metal/1L h-BN layers from the Ge substrate. The exfoliated film was immediately transferred to the freshly synthesized PEA_2SnI_4 film. To make conformal contacts, the film was gently pressed from the top with a soft elastomer. The TRT was detached by annealing the sample on a hot plate at 130 °C for 2 min while gently pressing it from the top. Post-annealing was then conducted at 130 °C in a glovebox for 2 h to further increase the conformal contact. To release the vdW contact, as described in Figure 2a, new TRT was attached onto the surface and then lifted. For the reference samples in Figures 1b and 4a, Al was thermally evaporated onto the as-grown PEA_2SnI_4 film directly with a thickness of 20 nm and a deposition rate of 0.1 Å/s. For CYTOP passivated samples, the CYTOP solution was spin-coated on top of the as-grown PEA_2SnI_4 film at 2000 rpm for 1 min, followed by annealing at 60 °C for 30 min to achieve a thickness of 1.2 μm. To deposit a 20 nm thick layer of Al_2O_3 on Al for the samples in Figures S6 and S8, atomic layer deposition (model: Plus 200, QUROS) was utilized.

https://doi.org/10.1021/acsenergylett.3c01195
ACS Energy Lett. 2023, 8, 3536−3544

PL Characterizations. Steady-state PL measurements were conducted using a confocal microscope in a reflection geometry (model: Alpha300RS, Witec). The excitation laser of 532 nm in wavelength was focused onto the sample by an objective of NA = 0.4. The focus of the objective and the tilting angle of the sample were carefully adjusted to maximize the reflected PL signals. The incident laser power was measured using a power meter (model: S170C & PM100D, Thorlabs) at the sample position. Unless otherwise specified, all PL measurements were conducted with an incident laser power density of 50 W/cm^2. To measure the temperature-dependent PL, the sample was placed in an optical cryostat (model: MPS-LN6C, Nextron).

Time-resolved PL was measured using a fluorescence lifetime spectrometer (model: Quantaurus-Tau, Hamamatsu) with an incident wavelength of 464 nm.

Other Characterizations. The UPS was measured (model: Nexsa, Thermo scientific) on the surface of as-grown perovskite films on metals (Au or Al) or fused silica. The samples, grown in a glovebox, were transferred to the UPS instrument without being exposed to ambient environment by using a portable vacuum container to maintain the pristine surfaces.

Ellipsometry was measured using an M-2000 instrument (J.A. Woollam) for the as-grown perovskite films on metal surfaces (Au or Al). Three different angles of incident light were used to measure phi and delta values for each perovskite film and bare metal substrates. The CompleteEASE program was used to extract complex refractive index values ($n + ik$) and film thickness by fitting using a spatial anisotropy model.

Absorption spectra were measured by UV−vis−NIR spectroscopy (model: V-770, Jasco) for the as-grown samples on fused silica substrates.

XRD measurements were conducted using a Panalytical X-ray diffractometer (model: Empyrean, Panalytical) for both the as-grown sample of PEA_2SnI_4 on fused silica and the sample of vdW Al/1L h-BN/PEA_2SnI_4/fused silica. Prior to the measurements, the upper PMMA layer was removed from the transferred vdW Al/1L h-BN film by using reactive ion etching with oxygen plasma (model: Vita, Femto Science) at 100 W for 5 min and repeated six times with an interval of 3 min between each etching process.

■ ASSOCIATED CONTENT

Supporting Information

The Supporting Information is available free of charge at https://pubs.acs.org/doi/10.1021/acsenergylett.3c01195.

XRD data before and after vdW contact, UV−vis absorption with PL spectrum, scheme of 1L h-BN mediated metal transfer process, ellipsometry with fitted n&k, calculation procedure and resultant parameters of relative PLQY, PL intensity on Al and Al_2O_3/Al, PL shift by vdW contact data, absolute PLQY data comparision with other measurement method, SRH recombination, fitted parameters of TRPL data, reported PLQY values with references (PDF)

■ AUTHOR INFORMATION

Corresponding Authors

Yong-Young Noh − *Department of Chemical Engineering, Pohang University of Science and Technology (POSTECH), Pohang 37673, Republic of Korea;* orcid.org/0000-0001-7222-2401; Email: yynoh@postech.ac.kr

Cheol-Joo Kim − *Department of Chemical Engineering, Pohang University of Science and Technology (POSTECH), Pohang 37673, Republic of Korea;* orcid.org/0000-0002-4312-3866; Email: kimcj@postech.ac.kr

Authors

Jun-Ho Park − *Department of Chemical Engineering, Pohang University of Science and Technology (POSTECH), Pohang 37673, Republic of Korea;* orcid.org/0000-0003-2887-1994

Youjin Reo − *Department of Chemical Engineering, Pohang University of Science and Technology (POSTECH), Pohang 37673, Republic of Korea*

Ju-Hyun Jung − *Department of Chemical Engineering, Pohang University of Science and Technology (POSTECH), Pohang 37673, Republic of Korea;* orcid.org/0000-0002-8283-621X

Taehyun Kim − *Department of Chemical Engineering, Pohang University of Science and Technology (POSTECH), Pohang 37673, Republic of Korea*

Taiho Park − *Department of Chemical Engineering, Pohang University of Science and Technology (POSTECH), Pohang 37673, Republic of Korea;* orcid.org/0000-0002-5867-4679

Complete contact information is available at: https://pubs.acs.org/10.1021/acsenergylett.3c01195

Notes

The authors declare no competing financial interest.

■ ACKNOWLEDGMENTS

This research was supported by the National R&D Program through the National Research Foundation of Korea (NRF) funded by the Ministry of Science and ICT (2020R1A4A1019455, 2023R1A2C2005427, 2022M3H4A1A01012718).

■ REFERENCES

(1) Liu, Y.; Dong, Y.; Zhu, T.; Ma, D.; Proppe, A.; Chen, B.; Zheng, C.; Hou, Y.; Lee, S.; Sun, B.; Jung, E. H.; Yuan, F.; Wang, Y.; Sagar, L. K.; Hoogland, S.; García de Arquer, F. P.; Choi, M.-J.; Singh, K.; Kelley, S. O.; Voznyy, O.; Lu, Z.-H.; Sargent, E. H. Bright and Stable Light-Emitting Diodes Based on Perovskite Quantum Dots in Perovskite Matrix. *J. Am. Chem. Soc.* **2021**, *143* (38), 15606−15615.

(2) Liu, Y.; Cui, J.; Du, K.; Tian, H.; He, Z.; Zhou, Q.; Yang, Z.; Deng, Y.; Chen, D.; Zuo, X.; Ren, Y.; Wang, L.; Zhu, H.; Zhao, B.; Di, D.; Wang, J.; Friend, R. H.; Jin, Y. Efficient Blue Light-Emitting Diodes Based on Quantum-Confined Bromide Perovskite Nanostructures. *Nat. Photonics* **2019**, *13* (11), 760−764.

(3) Zhang, D.; Zhang, Q.; Ren, B.; Zhu, Y.; Abdellah, M.; Fu, Y.; Cao, B.; Wang, C.; Gu, L.; Ding, Y.; Tsui, K.-H.; Fan, S.; Poddar, S.; Shu, L.; Zhang, Y.; Kuang, D.-B.; Liao, J.-F.; Lu, Y.; Zheng, K.; He, Z.; Fan, Z. Large-Scale Planar and Spherical Light-Emitting Diodes Based on Arrays of Perovskite Quantum Wires. *Nat. Photonics* **2022**, *16* (4), 284−290.

(4) Fox, M. *Optical Properties of Solids*, 2nd ed.; Oxford master series in physics; Oxford University Press: Oxford, U.K., 2010.

(5) Stranks, S. D.; Eperon, G. E.; Grancini, G.; Menelaou, C.; Alcocer, M. J. P.; Leijtens, T.; Herz, L. M.; Petrozza, A.; Snaith, H. J. Electron-Hole Diffusion Lengths Exceeding 1 Micrometer in an Organometal Trihalide Perovskite Absorber. *Science* **2013**, *342* (6156), 341−344.

(6) Han, T.-H.; Jang, K. Y.; Dong, Y.; Friend, R. H.; Sargent, E. H.; Lee, T.-W. A Roadmap for the Commercialization of Perovskite Light Emitters. *Nat. Rev. Mater.* **2022**, *7* (10), 757−777.
(7) Akkerman, Q. A.; Rainò, G.; Kovalenko, M. V.; Manna, L. Genesis, Challenges and Opportunities for Colloidal Lead Halide Perovskite Nanocrystals. *Nat. Mater.* **2018**, *17* (5), 394−405.
(8) du Fossé, I.; Mulder, J. T.; Almeida, G.; Spruit, A. G. M.; Infante, I.; Grozema, F. C.; Houtepen, A. J. Limits of Defect Tolerance in Perovskite Nanocrystals: Effect of Local Electrostatic Potential on Trap States. *J. Am. Chem. Soc.* **2022**, *144* (25), 11059−11063.
(9) ten Brinck, S.; Zaccaria, F.; Infante, I. Defects in Lead Halide Perovskite Nanocrystals: Analogies and (Many) Differences with the Bulk. *ACS Energy Lett.* **2019**, *4* (11), 2739−2747.
(10) Bodnarchuk, M. I.; Boehme, S. C.; ten Brinck, S.; Bernasconi, C.; Shynkarenko, Y.; Krieg, F.; Widmer, R.; Aeschlimann, B.; Günther, D.; Kovalenko, M. V.; Infante, I. Rationalizing and Controlling the Surface Structure and Electronic Passivation of Cesium Lead Halide Nanocrystals. *ACS Energy Lett.* **2019**, *4* (1), 63−74.
(11) Pitaro, M.; Tekelenburg, E. K.; Shao, S.; Loi, M. A. Tin Halide Perovskites: From Fundamental Properties to Solar Cells. *Adv. Mater.* **2022**, *34* (1), No. 2105844.
(12) Li, X.; Gao, X.; Zhang, X.; Shen, X.; Lu, M.; Wu, J.; Shi, Z.; Colvin, V. L.; Hu, J.; Bai, X.; Yu, W. W.; Zhang, Y. Lead-Free Halide Perovskites for Light Emission: Recent Advances and Perspectives. *Adv. Sci.* **2021**, *8* (4), No. 2003334.
(13) Zhang, T.; Zhou, C.; Feng, X.; Dong, N.; Chen, H.; Chen, X.; Zhang, L.; Lin, J.; Wang, J. Regulation of the Luminescence Mechanism of Two-Dimensional Tin Halide Perovskites. *Nat. Commun.* **2022**, *13* (1), 60.
(14) Kim, Y.-H.; Kim, S.; Kakekhani, A.; Park, J.; Park, J.; Lee, Y.-H.; Xu, H.; Nagane, S.; Wexler, R. B.; Kim, D.-H.; Jo, S. H.; Martínez-Sarti, L.; Tan, P.; Sadhanala, A.; Park, G.-S.; Kim, Y.-W.; Hu, B.; Bolink, H. J.; Yoo, S.; Friend, R. H.; Rappe, A. M.; Lee, T.-W. Comprehensive Defect Suppression in Perovskite Nanocrystals for High-Efficiency Light-Emitting Diodes. *Nat. Photonics* **2021**, *15* (2), 148−155.
(15) Lin, K.; Xing, J.; Quan, L. N.; de Arquer, F. P. G.; Gong, X.; Lu, J.; Xie, L.; Zhao, W.; Zhang, D.; Yan, C.; Li, W.; Liu, X.; Lu, Y.; Kirman, J.; Sargent, E. H.; Xiong, Q.; Wei, Z. Perovskite Light-Emitting Diodes with External Quantum Efficiency Exceeding 20 per Cent. *Nature* **2018**, *562* (7726), 245−248.
(16) Fang, Z.; Chen, W.; Shi, Y.; Zhao, J.; Chu, S.; Zhang, J.; Xiao, Z. Dual Passivation of Perovskite Defects for Light-Emitting Diodes with External Quantum Efficiency Exceeding 20%. *Adv. Funct. Mater.* **2020**, *30* (12), No. 1909754.
(17) Yang, X.; Ma, L.; Li, L.; Luo, M.; Wang, X.; Gong, Q.; Lu, C.; Zhu, R. Towards Micro-PeLED Displays. *Nat. Rev. Mater.* **2023**, *8*, 341.
(18) Kim, J. S.; Heo, J.-M.; Park, G.-S.; Woo, S.-J.; Cho, C.; Yun, H. J.; Kim, D.-H.; Park, J.; Lee, S.-C.; Park, S.-H.; Yoon, E.; Greenham, N. C.; Lee, T.-W. Ultra-Bright, Efficient and Stable Perovskite Light-Emitting Diodes. *Nature* **2022**, *611* (7937), 688−694.
(19) Treglia, A.; Ambrosio, F.; Martani, S.; Folpini, G.; Barker, A. J.; Albaqami, M. D.; De Angelis, F.; Poli, I.; Petrozza, A. Effect of Electronic Doping and Traps on Carrier Dynamics in Tin Halide Perovskites. *Mater. Horizons* **2022**, *9* (6), 1763−1773.
(20) Kheng, K.; Cox, R. T.; d' Aubigné, M. Y.; Bassani, F.; Saminadayar, K.; Tatarenko, S. Observation of Negatively Charged Excitons X^- in Semiconductor Quantum Wells. *Phys. Rev. Lett.* **1993**, *71* (11), 1752−1755.
(21) Huard, V.; Cox, R. T.; Saminadayar, K.; Arnoult, A.; Tatarenko, S. Bound States in Optical Absorption of Semiconductor Quantum Wells Containing a Two-Dimensional Electron Gas. *Phys. Rev. Lett.* **2000**, *84* (1), 187−190.
(22) Pelant, I.; Valenta, J. *Luminescence Spectroscopy of Semiconductors*; Oxford University Press, 2012. DOI: 10.1093/acprof:oso/9780199588336.001.0001.
(23) Petrozza, A. Doping of Soft Semiconductors. *ACS Energy Lett.* **2022**, *7* (3), 1101−1102.
(24) Amerling, E.; Lu, H.; Larson, B. W.; Maughan, A. E.; Phillips, A.; Lafalce, E.; Whittaker-Brooks, L.; Berry, J. J.; Beard, M. C.; Vardeny, Z. V.; Blackburn, J. L. A Multi-Dimensional Perspective on Electronic Doping in Metal Halide Perovskites. *ACS Energy Lett.* **2021**, *6* (3), 1104−1123.
(25) Yi, H. T.; Rangan, S.; Tang, B.; Frisbie, C. D.; Bartynski, R. A.; Gartstein, Y. N.; Podzorov, V. Electric-Field Effect on Photoluminescence of Lead-Halide Perovskites. *Mater. Today* **2019**, *28*, 31−39.
(26) Liu, C.; Huang, Z.; Hu, X.; Meng, X.; Huang, L.; Xiong, J.; Tan, L.; Chen, Y. Grain Boundary Modification via F4TCNQ To Reduce Defects of Perovskite Solar Cells with Excellent Device Performance. *ACS Appl. Mater. Interfaces* **2018**, *10* (2), 1909−1916.
(27) Zhu, H.; Liu, A.; Shim, K. I.; Hong, J.; Han, J. W.; Noh, Y.-Y. High-Performance and Reliable Lead-Free Layered-Perovskite Transistors. *Adv. Mater.* **2020**, *32* (31), No. 2002717.
(28) Heo, S.; Roh, K.; Zhang, F.; Tignor, S. E.; Bocarsly, A. B.; Kahn, A.; Rand, B. P. Electrochemically n-Doped $CsPbBr_3$ Nanocrystal Thin Films. *ACS Energy Lett.* **2022**, *7* (1), 211−216.
(29) Mulder, J. T.; du Fossé, I.; Alimoradi Jazi, M.; Manna, L.; Houtepen, A. J. Electrochemical p-Doping of $CsPbBr_3$ Perovskite Nanocrystals. *ACS Energy Lett.* **2021**, *6* (7), 2519−2525.
(30) Hansen, K. R.; McClure, C. E.; Powell, D.; Hsieh, H.-C.; Flannery, L.; Garden, K.; Miller, E. J.; King, D. J.; Sainio, S.; Nordlund, D.; Colton, J. S.; Whittaker-Brooks, L. Low Exciton Binding Energies and Localized Exciton−Polaron States in 2D Tin Halide Perovskites. *Adv. Opt. Mater.* **2022**, *10* (9), No. 2102698.
(31) Yuan, F.; Zheng, X.; Johnston, A.; Wang, Y.-K.; Zhou, C.; Dong, Y.; Chen, B.; Chen, H.; Fan, J. Z.; Sharma, G.; Li, P.; Gao, Y.; Voznyy, O.; Kung, H.-T.; Lu, Z.-H.; Bakr, O. M.; Sargent, E. H. Color-Pure Red Light-Emitting Diodes Based on Two-Dimensional Lead-Free Perovskites. *Sci. Adv.* **2020**, *6* (42), No. eabb0253.
(32) Milot, R. L.; Klug, M. T.; Davies, C. L.; Wang, Z.; Kraus, H.; Snaith, H. J.; Johnston, M. B.; Herz, L. M. The Effects of Doping Density and Temperature on the Optoelectronic Properties of Formamidinium Tin Triiodide Thin Films. *Adv. Mater.* **2018**, *30* (44), No. 1804506.
(33) Reo, Y.; Zhu, H.; Liu, A.; Noh, Y.-Y. Molecular Doping Enabling Mobility Boosting of 2D Sn2+-Based Perovskites. *Adv. Funct. Mater.* **2022**, *32* (38), No. 2204870.
(34) Reo, Y.; Zhu, H.; Go, J.-Y.; In Shim, K.; Liu, A.; Zou, T.; Jung, H.; Kim, H.; Hong, J.; Han, J. W.; Noh, Y.-Y. Effect of Monovalent Metal Iodide Additives on the Optoelectric Properties of Two-Dimensional Sn-Based Perovskite Films. *Chem. Mater.* **2021**, *33* (7), 2498−2505.
(35) Yang, S.-J.; Jung, J.-H.; Lee, E.; Han, E.; Choi, M.-Y.; Jung, D.; Choi, S.; Park, J.-H.; Oh, D.; Noh, S.; Kim, K.-J.; Huang, P. Y.; Hwang, C.-C.; Kim, C.-J. Wafer-Scale Programmed Assembly of One-Atom-Thick Crystals. *Nano Lett.* **2022**, *22* (4), 1518−1524.
(36) Wang, Y.; Wan, Z.; Qian, Q.; Liu, Y.; Kang, Z.; Fan, Z.; Wang, P.; Wang, Y.; Li, C.; Jia, C.; Lin, Z.; Guo, J.; Shakir, I.; Goorsky, M.; Duan, X.; Zhang, Y.; Huang, Y.; Duan, X. Probing Photoelectrical Transport in Lead Halide Perovskites with van Der Waals Contacts. *Nat. Nanotechnol.* **2020**, *15* (9), 768−775.
(37) Schmidt, T.; Lischka, K.; Zulehner, W. Excitation-Power Dependence of the near-Band-Edge Photoluminescence of Semiconductors. *Phys. Rev. B* **1992**, *45* (16), 8989−8994.
(38) Park, J.-H.; Yang, S.-J.; Choi, C.-W.; Choi, S.-Y.; Kim, C.-J. Pristine Graphene Insertion at the Metal/Semiconductor Interface to Minimize Metal-Induced Gap States. *ACS Appl. Mater. Interfaces* **2021**, *13* (19), 22828−22835.
(39) Liu, Y.; Guo, J.; Zhu, E.; Liao, L.; Lee, S.-J.; Ding, M.; Shakir, I.; Gambin, V.; Huang, Y.; Duan, X. Approaching the Schottky−Mott Limit in van Der Waals Metal−Semiconductor Junctions. *Nature* **2018**, *557* (7707), 696−700.

(40) Zhou, Y.; Poli, I.; Meggiolaro, D.; De Angelis, F.; Petrozza, A. Defect Activity in Metal Halide Perovskites with Wide and Narrow Bandgap. *Nat. Rev. Mater.* **2021**, *6*, 986.
(41) Seitz, M.; Meléndez, M.; Alcázar-Cano, N.; Congreve, D. N.; Delgado-Buscalioni, R.; Prins, F. Mapping the Trap-State Landscape in 2D Metal-Halide Perovskites Using Transient Photoluminescence Microscopy. *Adv. Opt. Mater.* **2021**, *9* (18), No. 2001875.
(42) Chernikov, A.; van der Zande, A. M.; Hill, H. M.; Rigosi, A. F.; Velauthapillai, A.; Hone, J.; Heinz, T. F. Electrical Tuning of Exciton Binding Energies in Monolayer WS_2. *Phys. Rev. Lett.* **2015**, *115* (12), No. 126802.
(43) Kahmann, S.; Meggiolaro, D.; Gregori, L.; Tekelenburg, E. K.; Pitaro, M.; Stranks, S. D.; De Angelis, F.; Loi, M. A. The Origin of Broad Emission in ⟨100⟩ Two-Dimensional Perovskites: Extrinsic vs Intrinsic Processes. *ACS Energy Lett.* **2022**, *7* (12), 4232−4241.
(44) Maity, P.; Yin, J.; Cheng, B.; He, J.-H.; Bakr, O. M.; Mohammed, O. F. Layer-Dependent Coherent Acoustic Phonons in Two-Dimensional Ruddlesden−Popper Perovskite Crystals. *J. Phys. Chem. Lett.* **2019**, *10* (17), 5259−5264.
(45) Thouin, F.; Valverde-Chávez, D. A.; Quarti, C.; Cortecchia, D.; Bargigia, I.; Beljonne, D.; Petrozza, A.; Silva, C.; Srimath Kandada, A. R. Phonon Coherences Reveal the Polaronic Character of Excitons in Two-Dimensional Lead Halide Perovskites. *Nat. Mater.* **2019**, *18* (4), 349−356.
(46) Monreal, R. C. Electron-Phonon Interaction in the Dynamics of Trap Filling in Quantum Dots. *Phys. Rev. B* **2021**, *104* (18), No. 184304.
(47) Kahmann, S.; Duim, H.; Fang, H.-H.; Dyksik, M.; Adjokatse, S.; Rivera Medina, M.; Pitaro, M.; Plochocka, P.; Loi, M. A. Photophysics of Two-Dimensional Perovskites—Learning from Metal Halide Substitution. *Adv. Funct. Mater.* **2021**, *31* (46), No. 2103778.
(48) Yu, S.; Xu, J.; Shang, X.; Ma, E.; Lin, F.; Zheng, W.; Tu, D.; Li, R.; Chen, X. Unusual Temperature Dependence of Bandgap in 2D Inorganic Lead-Halide Perovskite Nanoplatelets. *Adv. Sci.* **2021**, *8* (19), No. 2100084.
(49) "Chemical and Physical Properties". Phenethylamine. PubChem Compound. United States National Library of Medicine − National Center for Biotechnology Information. https://pubchem.ncbi.nlm.nih.gov/compound/1001?from=summary#section=Chemical-and-Physical-Properties (accessed 2023−03−13).
(50) Liang, A.; Gao, Y.; Asadpour, R.; Wei, Z.; Finkenauer, B. P.; Jin, L.; Yang, J.; Wang, K.; Chen, K.; Liao, P.; Zhu, C.; Huang, L.; Boudouris, B. W.; Alam, M. A.; Dou, L. Ligand-Driven Grain Engineering of High Mobility Two-Dimensional Perovskite Thin-Film Transistors. *J. Am. Chem. Soc.* **2021**, *143* (37), 15215−15223.
(51) Cho, C.; Feldmann, S.; Yeom, K. M.; Jang, Y.-W.; Kahmann, S.; Huang, J.-Y.; Yang, T. C.; Khayyat, M. N. T.; Wu, Y.-R.; Choi, M.; Noh, J. H.; Stranks, S. D.; Greenham, N. C. Efficient Vertical Charge Transport in Polycrystalline Halide Perovskites Revealed by Four-Dimensional Tracking of Charge Carriers. *Nat. Mater.* **2022**, *21* (12), 1388−1395.
(52) Proppe, A. H.; Johnston, A.; Teale, S.; Mahata, A.; Quintero-Bermudez, R.; Jung, E. H.; Grater, L.; Cui, T.; Filleter, T.; Kim, C.-Y.; Kelley, S. O.; De Angelis, F.; Sargent, E. H. Multication Perovskite 2D/3D Interfaces Form via Progressive Dimensional Reduction. *Nat. Commun.* **2021**, *12* (1), 3472.
(53) Kwon, S.-J.; Ahn, S.; Heo, J.-M.; Kim, D. J.; Park, J.; Lee, H.-R.; Kim, S.; Zhou, H.; Park, M.-H.; Kim, Y.-H.; Lee, W.; Sun, J.-Y.; Hong, B. H.; Lee, T.-W. Chemically Robust Indium Tin Oxide/Graphene Anode for Efficient Perovskite Light-Emitting Diodes. *ACS Appl. Mater. Interfaces* **2021**, *13* (7), 9074−9080.

https://doi.org/10.1021/acsenergylett.3c01195
ACS Energy Lett. 2023, 8, 3536−3544